Available online at www.sciencedirect.com
ScienceDirect
Polymer 48 (2007) 7364–7373
polymer
www.elsevier.com/locate/polymer

Conformation transition and molecular mobility of isolated poly(ethylene oxide) chains confined in urea nanochannels

Hai-Mu Ye [a], Min Peng [b], Jun Xu [a,*], Bao-Hua Guo [a], Qun Chen [b], Tian-Liang Yun [c,d], Hui Ma [c,d]

[a] *Institute of Polymer Science & Engineering, Department of Chemical Engineering, Tsinghua University, Beijing 100084, China*
[b] *Physics Department and Shanghai Key Laboratory for Functional Magnetic Resonance Imaging, East China Normal University, Shanghai 200062, China*
[c] *Department of Physics, Tsinghua University, Beijing 100084, China*
[d] *Graduate School at Shenzhen, Tsinghua University, Shenzhen 518055, China*

Received 6 July 2007; received in revised form 17 October 2007; accepted 23 October 2007
Available online 26 October 2007

Abstract

Inclusion compounds formed from host small molecules and guest polymers have provided a novel platform to study the behavior of isolated polymer chains confined in nanochannels. In this article, the PEO chain conformation in the metastable poly(ethylene oxide) (PEO)–urea inclusion compound (IC) and its transition was characterized via a combination of different analytical methods. Based on the FTIR and Raman spectroscopy results, PEO chains in the metastable tetragonal IC are tentatively assigned to the *tgg′* conformation. The structural changes of the metastable tetragonal IC to the stable trigonal form were observed via *in situ* FTIR and *ex situ* WAXD. The transformation is a kinetic solid–solid process and can even occur at room temperature. The activation energy of about 222 kJ/mol indicates that the transition occurred via cooperative disruption of several hydrogen bonds. Measurement of the laboratory frame spin-lattice relaxation time T_1 (^{13}C) shows that molecular motions of the nanoconfined PEO chains are more intensive than the neat crystalline PEO but weaker than those of the neat amorphous PEO. Second harmonic generation microscopy demonstrates that the trigonal IC exhibits stronger nonlinear optical activity than the tetragonal IC. The intermolecular hydrogen bonding is attributed to the driving force for the transformation of the metastable tetragonal IC into the stable trigonal form.

Keywords: Inclusion compound; Chain conformation; ^{13}C spin-lattice relaxation time

1. Introduction

More attention has been paid on the nanoconfined polymer chains because they show distinct different conformations from the bulk polymers. It will be of particular interest when each strand of polymer chains is separately confined in the nanochannels formed by another component. Extensive studies [1–5] have focused on reeling of polymers into the preformed nanotubes. However, since the process leads to dramatic decrease of the entropy of the polymers, special interaction of the polymer chains with the confining environment is necessary to obtain negative ΔG of the system. Due to the low diffusion coefficient of macromolecules into the nanochannels, the load capacity is usually unsatisfying [6]. Furthermore, it is quite a challenge to obtain nanochannels with narrow size distribution. On the contrary, the crystalline inclusion compounds (ICs) [1,7–10] formed from spontaneous assembly of polymers and small molecules provide a new method for observing the behaviors of isolated nanoconfined polymer chains. The ICs can be obtained in sufficient amount so that the common analytical methods are feasible to characterize the material structures. Various ICs of polymers and small molecules, such as urea [9–17], perhydrotriphene [1,18] and cyclodextrin [1,2,4], have been reported, in

* Corresponding author. Tel./fax: +86 10 6278 4550.
E-mail address: jun-xu@mail.tsinghua.edu.cn (J. Xu).

0032-3861/$ - see front matter © 2007 Elsevier Ltd. All rights reserved.
doi:10.1016/j.polymer.2007.10.033

which the included polymer chains are confined by the nanochannels composed of the small molecules, or the host clathrates. In the polymer–urea inclusion compounds, the polymer chains are extended and separated from neighboring chains by the channels of about 5.5 Å diameter [1,19]. Among them, the PEO–urea IC has attracted much interest due to the following reasons: first, there are at least two types of crystal modifications; second, melt crystallization is allowed because the melting temperature is lower than the degradation temperature; third, hydrogen bonding is a key factor affecting the crystallization behavior.

Up to now, three crystalline modifications have been observed in PEO–urea ICs, which depend on the crystallization condition. The IC formed from solution took a trigonal crystal structure [13,20], in which PEO segments adopted an approximate 4_1 helix conformation; while recrystallization from melt produced a hexagonal form [13]. The ethylene oxide oligomer (PEG)–urea inclusion compounds were found to crystallize in two crystalline modifications, tetragonal and hexagonal form. The tetragonal form contained eight molecules of urea and eight ethylene oxide units in a unit cell, which transformed into the trigonal form on heating [15]. Bogdanov et al. [14,21] studied both the solid and molten states of PEO–urea IC via infrared spectroscopy and observed the transformation of the metastable IC into the stable form when heated to 85–90 °C; however, the crystalline structure and the chain conformation in the metastable form have not been assigned yet. Solid state ^{13}C NMR has been applied to determine the mobility of polymer chains in the trigonal PEO–urea IC. The measured spin-lattice relaxation time showed that the included polymer chains demonstrated higher mobility than the bulk crystalline polymer chains [1,13].

Though much work has been carried out on PEO–urea IC, however, there are still some items unsolved, e.g. the PEO conformation, the chain mobility in the metastable crystalline modification and the details of the transition of the crystal modification have not yet been clarified. In addition, urea has been found to show nonlinear optical (NLO) behavior; nonetheless, the NLO behavior of the polymer–urea complex has not been reported so far.

In the present work, the crystalline structure, PEO conformation, kinetics of the transition process and the PEO mobility in the metastable tetragonal ICs are clarified via a combination of different methods, such as polarized optical microscopy (POM), differential scanning calorimetry (DSC), Fourier transform infrared spectroscopy (FTIR), Raman spectroscopy, wide angle X-ray diffraction (WAXD) and solid state ^{13}C NMR. Furthermore, second harmonic generation (SHG) microscopy was introduced to characterize the nonlinear optical property of the different crystal modifications of the ICs for the first time.

2. Experimental part

2.1. Sample preparation

PEO with Mw of about 1×10^6 was obtained from Shanghai Lianshen Chemical Company. The solution-grown PEO–urea IC crystals were obtained from the dilute (0.5%, w/v) water solution of PEO and urea using a freezing drier after the solution had been frozen in a −20 °C refrigerator. There were no water molecules in the ICs, since the ICs prepared from freeze drying showed the same IR spectra as the samples cocrystallized from the supersaturated methanol solution.

2.2. POM

The inclusion compound was melted between two clean glass slides at 160 °C and held for 2 min, then transferred quickly to a thermal stage preset at a fixed temperature for isothermal crystallization. After impingement of the spherulites and no observable changes occurred, the digital images of the spherulites were captured with a computer controlled charge coupled detector (Tota, Japan). To obtain qualitative information of birefringence, a first order tint plate (530 nm) was inserted into the illumination path.

2.3. DSC

DSC-60 calorimeter (Shimadzu, Japan) was employed in the calorimetric analysis of pure PEO, urea and PEO–urea IC. Sample about 3 mg was held in aluminum seal during each process at a heating rate of 10 °C/min and an indium standard was used for calibration. The endothermic peak temperature was taken as melting point.

2.4. X-ray diffraction

Wide angle X-ray diffractions of the disk-shaped samples of about 5 mm in diameter and 0.5 mm in thickness were recorded at ambient conditions on a BRUKER D8 Advance instrument using Ni-filtered Cu Kα radiation. The supplied power was 3 kW. The scanning was carried out with 2θ from 2° to 50° with a step of 0.02°, and the diffraction peak positions of the sample were calibrated from the pattern of aluminum.

2.5. FTIR

The PEO–urea IC film was sandwiched between KBr windows. FTIR spectra were recorded on a Nicolet-560 IR spectrometer by signal averaging over 32 scans at a resolution of 4 cm^{-1} in the wavenumber range of 4000–400 cm^{-1}. To reveal the details of transformation of the crystals, *in situ* FTIR study was carried out. The thin film sandwiched between KBr windows was placed in a manually controlled heater. The tetragonal PEO–urea ICs were kept at a fixed temperature for a long period of time and the FTIR spectrum was recorded for every 2 or 3 min.

2.6. Raman spectroscopy

A Renishaw RM-2000 micro-Raman spectrometer was used to obtain the Raman spectra of the samples at the excitation wavelength of 633 nm. The spectrometer operates in 180°

backscattering geometry and utilizes a grating of 1800 lines/mm. The resolution is 1 cm^{-1}. A 50× objective lens with a numerical aperture of 0.5 is used to collect backscattering light and, accordingly, the radius of laser spot is 0.65 μm. The Raman spectrum was obtained via six accumulations of the backscattering light, each lasting for 30 s. The laser power irradiated on the sample is 4.7 mW.

2.7. Solid state ^{13}C NMR

High-resolution solid state ^{13}C NMR experiments were performed on a Bruker DSX-300 spectrometer operating at 75.47 MHz at room temperature. ^{13}C spectra were all acquired by employing the combination of cross-polarization (CP), magic-angle spinning (MAS) and high-power dipolar decoupling (DD) techniques. The acquisition parameters were as follows: MAS rate, 5 kHz; recycle delay, 5 s; contact time for CP, 0.2 ms; ^{1}H decoupling field strength, 62.5 kHz; number of accumulations, 1024. The ^{13}C chemical shifts were determined from the carbonyl carbon signal (176.03 ppm) of glycine relative to tetramethylsilane (TMS). ^{13}C spin-lattice relaxation time T_1 was determined by a CP based inversion-recovery pulse sequence.

2.8. Second harmonic generation microscopy

A two-photon fluorescence microscope (BioRad MRC1024 MP) was used for SHG imaging. The light source was a Ti–Sapphire femto second laser system (Millennium V pumped Tsunami Lite, Spectra Physics), which provided ~120 fs polarized short pulses at 80 MHz rep rate and 810 nm wavelength. Optics for the transmission imaging channel was replaced with an extra detection channel for forward propagating SHG. A 10 nm pass-band filter centered at 405 nm was used to filter through the narrow band SHG, and a high OD blocking filter was used to reject the two-photon fluorescence and, more importantly, the 810 nm fundamental laser light.

3. Results and discussion

3.1. Crystalline structure of the inclusion compounds

After melting, the PEO–urea inclusion compound (IC) was isothermally crystallized at different temperatures ranging from room temperature to 110 °C. In the crystallized film, the PEO–urea IC can exist as two types of crystals: when crystallized at the temperatures higher than 70 °C, only the stable form with positive spherulites were observed (Fig. 1a); while crystallized at temperatures lower than 70 °C, the metastable form appeared as small crystal grains or negative spherulites besides the stable form. When the melt was quenched to liquid nitrogen temperature, the metastable form was predominantly observed (Fig. 1b). By adjusting the crystallization condition, the two types of crystals with occupation area larger than 5×5 mm^2 could be separately obtained, which were used for further DSC, WAXD, FTIR, Raman and solid state ^{13}C NMR studies. Real-time POM was carried out during heating to reveal the melting process of the different crystalline modifications. While heating to 65–90 °C, the metastable form transformed into another form, which finally melted in the range of 136–140 °C. The stable form melted at about 140 °C as well.

DSC curves of the two types of crystals were recorded during heating at a rate of 10 °C/min. Two endothermic peaks at ca. 71 °C and 141 °C were observed for the metastable form of the PEO–urea IC (Fig. 2, curve a), while only one endotherm at 141 °C appeared for the stable form (Fig. 2, curve b). To reveal the origin of the endotherm at 71 °C, annealing of the metastable IC samples were carried out at 60 °C for 0, 1, and 3 h, respectively. Fig. 3 shows the DSC results of the annealed ICs. The endothermic peak at around 71 °C decreased with annealing time and almost disappeared after annealing for 3 h, which confirms that the endothermic peak at 71 °C corresponds to the metastable form.

Both POM observation and DSC study indicate that the metastable form transforms into the stable form on heating. The transition has been reported by Bogdanov et al.'s [14] and Suehiro and Nagano's studies [15], though different transition temperature was observed, which may be due to the different preparation method of the PEO–urea ICs. In the previous reports [14,15] the PEO–urea ICs were all produced by cocrystallization from the supersaturated methanol solution; while in this article the ICs were produced from freeze drying of the water solution.

To reveal the microscopic crystalline structure of the two types of PEO–urea ICs, WAXD study was performed, with the results shown in Fig. 4. The diffractograms of the metastable form (curve a) and the stable form (curve b) are quite different. The latter is indexed into a trigonal unit cell with the crystal lattice parameters $a = b = 10.51$ Å and $c = 9.28$ Å, which are close to the result of Chenite and Brisse's work [20], in which $a = b = 10.52$ Å and $c = 9.26$ Å (measured at room temperature).

The diffractions of the metastable form are indexed into a tetragonal unit cell with the lattice parameters as follows: $a = b = 9.30$ Å, $c = 19.51$ Å. This is different from the previous report [13] that the high-Mw PEO–urea IC melt crystallized at room temperature produced hexagonal modification. Nevertheless, the unit cell parameters of the tetragonal modification of the high-Mw PEO–urea IC agree with the results of Suehiro and Nagano's [15] and Tonelli et al.'s work [13] on low-Mw (Mw = 400) PEG–U IC. The unit cell dimension of tetragonal PEO–urea IC is much larger than that of bulk urea, which is also tetragonal with $a = b = 5.58$ Å. The difference is due to the insertion of PEO molecules in the clathrates. From Fig. 4, it is observed that the sample is not 100% phase pure. The tetragonal IC sample contained trace amount of trigonal IC and vice versa. Our interpretation is that crystallization of the IC at around 70 °C was very fast, so that the quenched sample still contained trace amount of trigonal IC, which was formed at high temperature. When the IC melt was isothermally crystallized at high temperatures, crystallization was not complete, after cooled to room temperature,

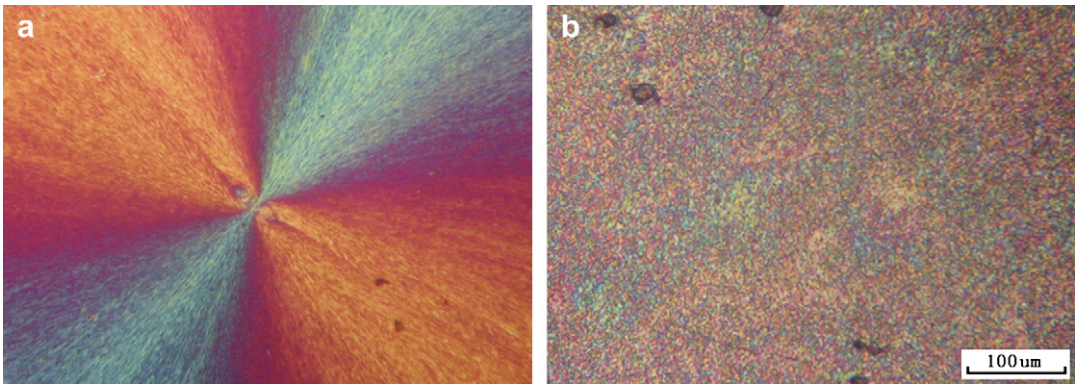

Fig. 1. Polarized optical micrographs of the stable form (a) and the metastable form (b) of the PEO–urea inclusion compound.

a small amount of amorphous melt further crystallized to form tetragonal IC.

Fig. 5 shows the WAXD diffractograms of PEO–urea ICs after annealing for different periods of time. The curve (a) belongs to the as-prepared metastable tetragonal IC, and the curves (b)–(d) indicate the diffractograms of the same sample after annealing at 60 °C for 1 h, 3 h, and after further annealed at 70 °C for 12 h, respectively. Comparing the four diffractograms, we can find that the intensities of the peaks at 21.16° and 22.36° due to the (202) and (114) planes of the tetragonal form gradually decrease, and the intensity of the peak at 21.74° due to the (201) plane of the trigonal form increases with the thermal treatment (see Fig. 5(b)–(d)). Fig. 5 further confirms that the crystals of PEO–urea IC transit from the tetragonal into the trigonal form during annealing.

3.2. PEO conformation in the inclusion compounds

Fourier transform infrared spectroscopy (FTIR) and Raman spectroscopy are effective tools to reveal the conformation of polymer chains. Fig. 6 shows the FTIR spectra of PEO–urea IC melt, the tetragonal and the trigonal crystalline forms. The latter two types of ICs demonstrate quite different IR spectra, suggesting different PEO chain conformations.

PEO chains in the trigonal modification adopted 4_1 helical conformation $(tgt)_4$, as reported by Chenite and Brisse [20]. The bands at 1360, 1279, 1248, 948 and 843 cm^{-1} bands are assigned to CH_2 wagging, CH_2 twisting, CH_2 rocking, CH_2 rocking and CH_2–O–CH_2 deformation of the *gauche* conformation, respectively. The bands at 1342 and 964 cm^{-1} are assigned to CH_2 wagging, CH_2 twisting and CH_2 rocking of the *trans* conformation, respectively [22,23].

The IR bands of the PEO chains in the tetragonal IC are quite different from those in the trigonal IC. New bands at 1350, 1307, 1242, 931 and 848 cm^{-1} were observed in the tetragonal IC. FTIR bands in the range of 1314–1325 cm^{-1}, though much weaker than that reported here, were previously observed in PEO inserted into the interlamellar space of intercalated $CdPS_3$ [24], homoionic NH_4^+-smectites [25] and layered double hydroxides [26], which were assigned to the

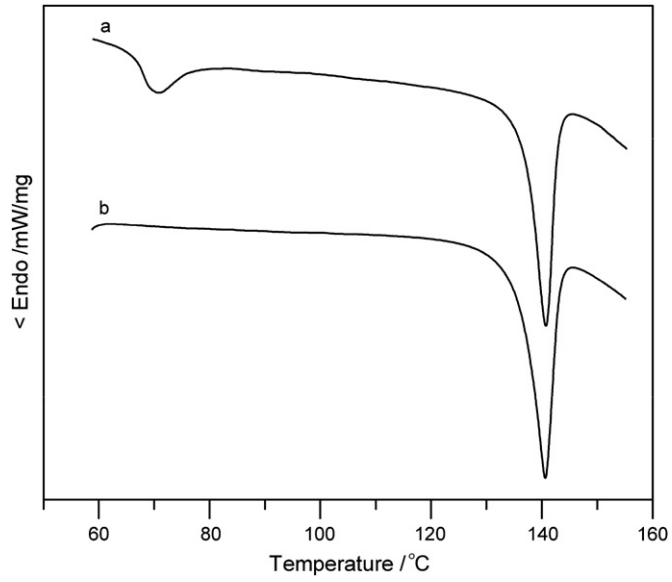

Fig. 2. DSC curves of PEO–urea IC: (a) the metastable form and (b) the stable form.

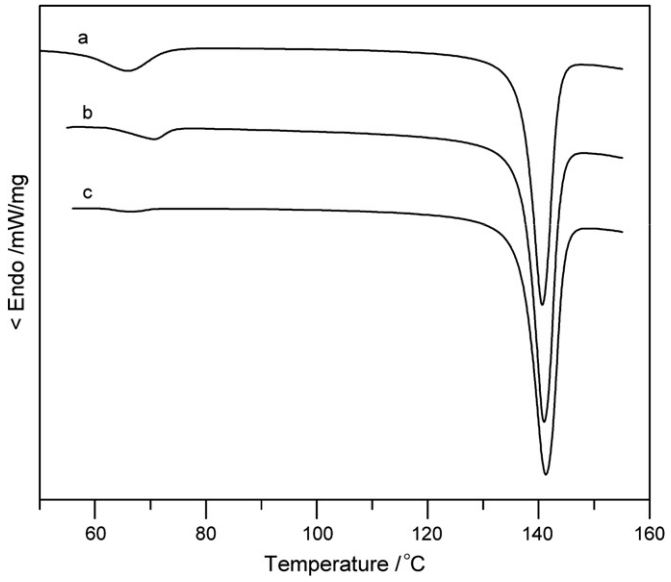

Fig. 3. DSC curves of the PEO–urea IC crystals obtained via annealing of the original metastable form at 60 °C for (a) 0 h; (b) 1 h, and (c) 3 h.

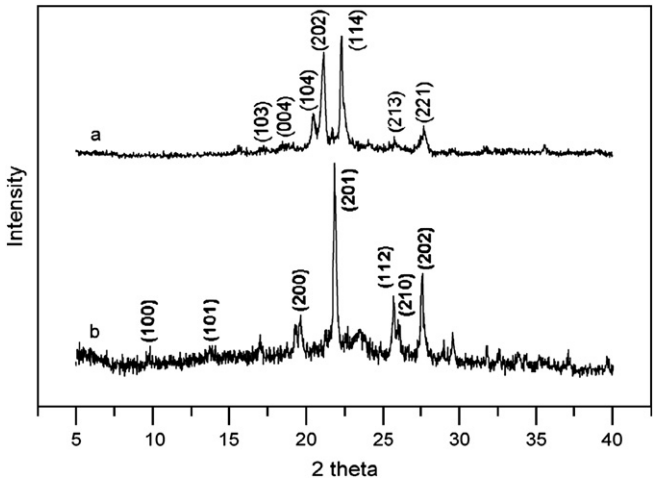

Fig. 4. X-ray diffractograms of PEO–urea IC: (a) the metastable form, and (b) the stable form.

$\delta(CH_2)$ vibration mode of *trans* $O-CH_2-CH_2-O$ conformation. It was also reported that in the stretched PEO film the chains adopted *ttt* conformation [27]. To see whether the 1307 cm^{-1} band arised from *trans* $O-CH_2-CH_2-O$ conformation, we recorded the FTIR spectrum of a uniaxially stretched PEO film; however, no bands were observed in the range of 1300–1330 cm^{-1} (data not shown here). Consequently, it is not plausible to assign the band around 1307 cm^{-1} to the *trans* zigzag or *ttt* conformation.

To further assign the chain conformation of PEO in the ICs, Raman spectroscopy of the two types of ICs was further investigated, and the result is presented in Fig. 7. The strongest

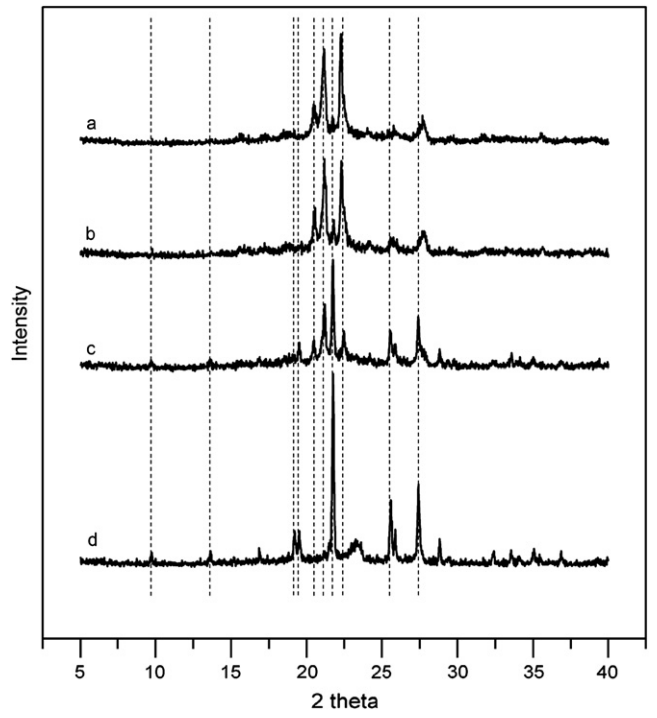

Fig. 5. *In situ* X-ray diffraction patterns of PEO–urea IC (a) the as-prepared metastable tetragonal IC; (b) annealed at 60 °C for 1 h; (c) annealed at 60 °C for 3 h; (d) annealed at 60 °C for 3 h and further annealed at 70 °C for 12 h.

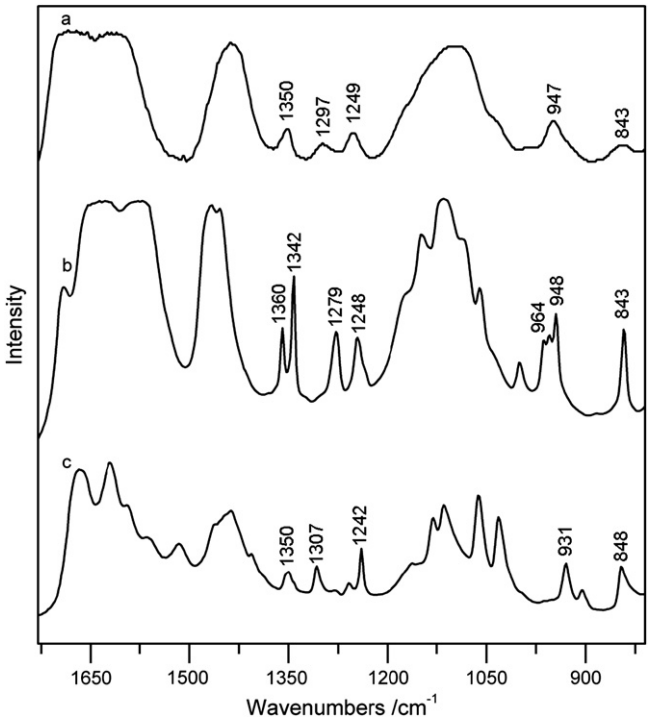

Fig. 6. Fourier transform infrared spectra in the region from 1700 to 800 cm^{-1} of the melt IC (a), the stable trigonal IC (b), and the metastable tetragonal IC (c).

band at 1008 cm^{-1} belongs to the urea clathrate. The trigonal IC shows Raman bands at 1278, 1237, 862 and 845 cm^{-1}, similar to the neat crystallized PEO. The tetragonal IC demonstrates bands at 1308, 1259 and 845 cm^{-1}. The strong bands in the range of 800–900 cm^{-1} arise from the backbone

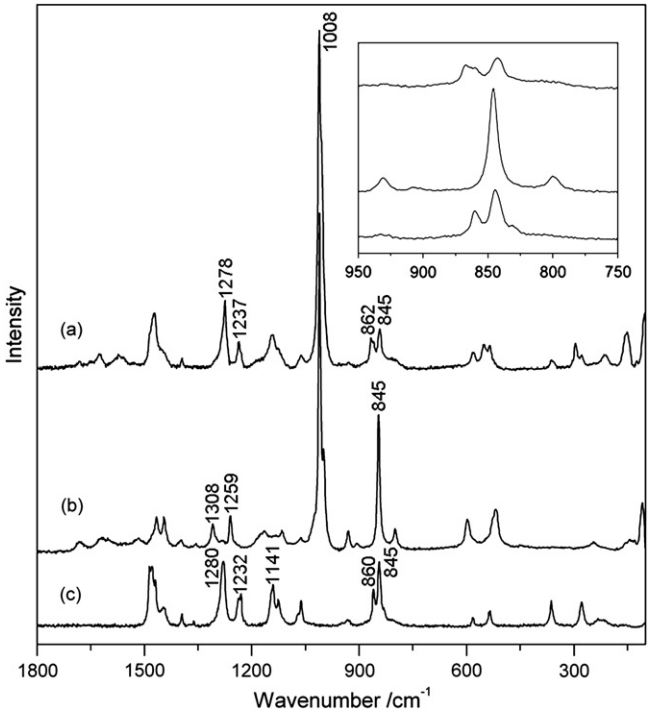

Fig. 7. Raman spectroscopy of (a) trigonal PEO–urea IC; (b) tetragonal PEO and (c) crystallized neat PEO. The inset shows the Raman spectroscopy from 950 to 750 cm^{-1}.

stretching vibration of PEO and are used for assignment of the chain conformation. Yang et al. reported simulation on Raman spectroscopy of different PEO conformations [28]: ''for the backbone stretching mode, the *tgttgttgt* and *tggtggtgg* sequences have a strong simulated band around 860 cm^{-1}, the $tgg'tgg'tgg'$ sequence has one at 830 cm^{-1}, and the *ttttttttt* and *ttgttgttg* sequences lack a substantial contributor in the 850 cm^{-1} region''. Consequently, we tentatively assign the predominant PEO conformation in the tetragonal PEO–urea IC to tgg'. Shift of the Raman peak may result from the effect of molecular weight and confinement. Yang's simulation results were obtained from 1,2-dimethoxyethane, while in this article the PEO chains are of high molecular weight of about 10^6 confined in the nanochannels. Based on both the IR and Raman spectroscopy, we tentatively suggest that the band at 1307 cm^{-1} in the PEO complexes correspond to the *gauche* conformation of $O-CH_2-CH_2-O$ units rather than the previous assigned all *trans* conformation [24–26]. Furthermore, our assignment agrees with the density functional simulation of vibrations of 1,2-dimethoxyethane [29], which shows that tgg' instead of *ttt* and *tgt* conformations has vibration at 1312–1301 cm^{-1}.

3.3. Transformation of the metastable tetragonal IC

To get a deeper insight, real-time FTIR was employed to study the transformation process of the metastable tetragonal form and to determine the kinetics at different temperatures. Fig. 8 shows the FTIR results at 60 °C. Significant changes can be observed during the transition process. Before the transformation, the PEO chains in the metastable tetragonal IC adopt tgg' conformation, with strong bands at 1307, 1242, 931 and 848 cm^{-1}. When kept at 60 °C, the tgg' conformation of $O-CH_2-CH_2-O$ gradually converted into the *tgt* conformation with bands at 1277, 1248, 948 and 843 cm^{-1}. Appearance of the peak at 1691 cm^{-1} (Fig. 8(c)) indicates a transformation of the crystal structure from tetragonal to trigonal modification. The reason for this peak's appearance is the existence of some isolated urea molecules in the channels of the trigonal IC [13]. It can be found that the 1350 cm^{-1} (amorphous) band does not completely disappear after the transition. The appearance of 1247 cm^{-1} band results from the overlap of the broad 1242 cm^{-1} band of amorphous PEO and the narrow 1248 cm^{-1} band of 4_1 helix. Fig. 9 compares the final spectrum after transition to the calculated spectrum

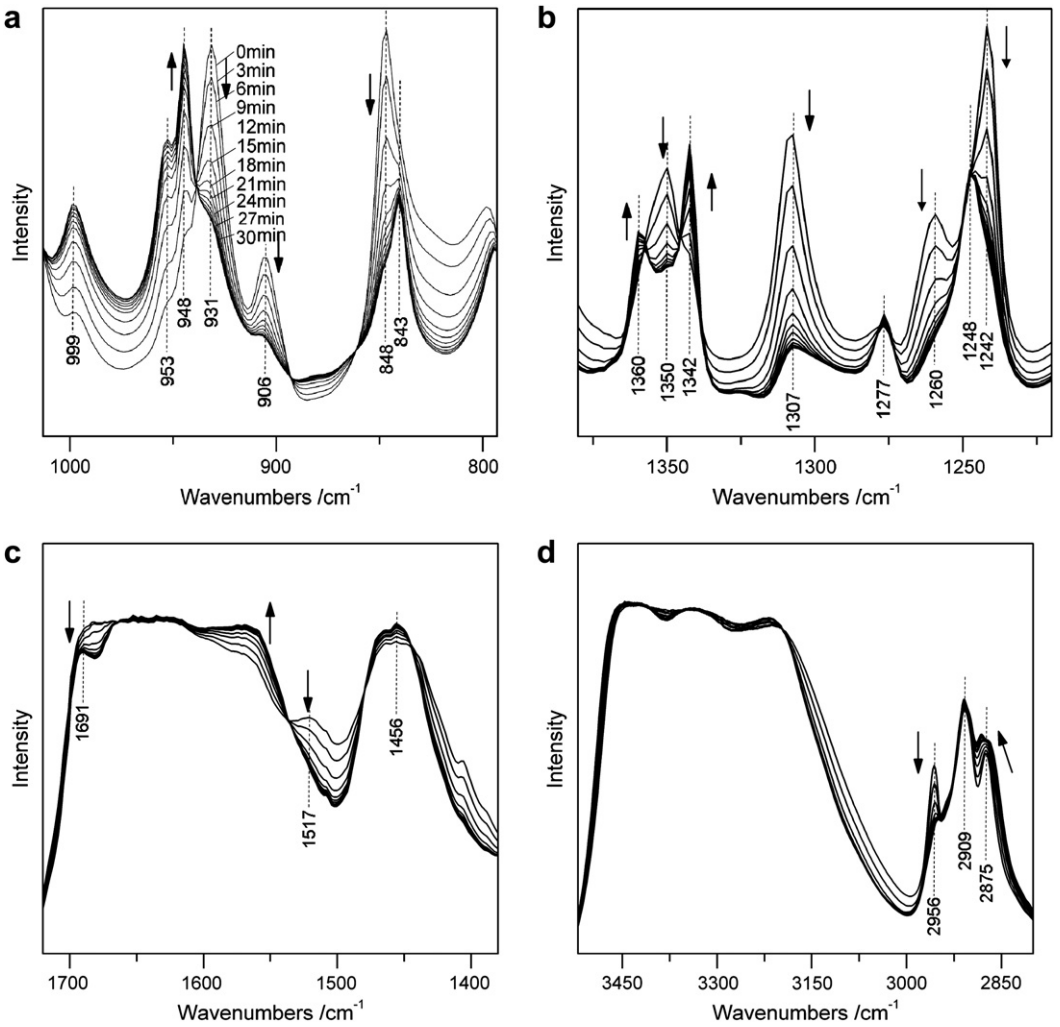

Fig. 8. The *in situ* FTIR spectra of PEO–urea IC transformation at 60 °C. The time interval of two consecutive records is 3 min.

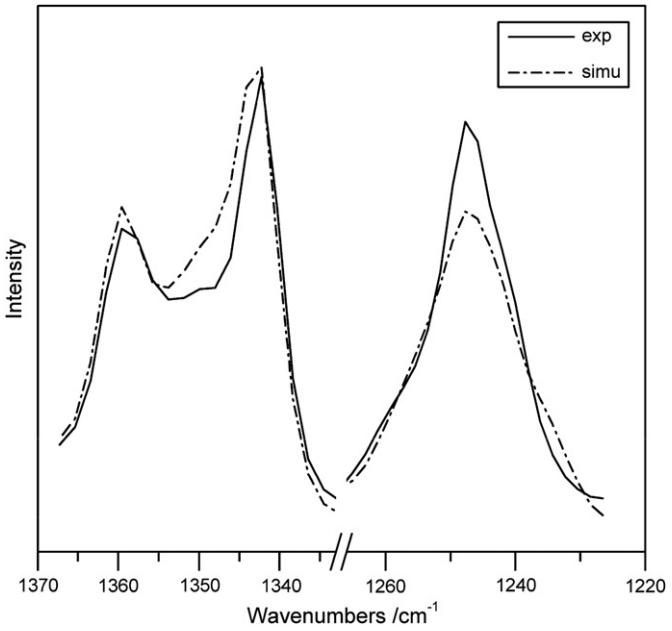

Fig. 9. Comparison of the final spectrum of transition (exp) and the calculated spectrum (simu) from linear sum of 4_1 helix (curve b in Fig. 6) and the amorphous conformation (curve c in Fig. 6).

from linear sum of 4_1 helix and the amorphous conformation (using the IR band of the amorphous IC melt). The two spectra match well, which suggests that during the transition the confined *tgg′* PEO chains in the tetragonal IC gradually change into 4_1 helical and the random amorphous conformation, as schemed in Fig. 10. It has been reported that the molar ratio of [urea]/[CH_2CH_2O] is 1.0 in tetragonal form while 1.8 in trigonal form of PEG–U IC and PEO–urea IC [15,20]. During the transition, in order to satisfy the higher urea ratio consumption, some PEO chains escaped from the urea channels to form the random amorphous fraction.

Fig. 11 shows the conversion of the tetragonal form at 50 °C, 60 °C and 70 °C, measured by FTIR (using the relative area change of peak at 1307 cm^{-1}). The transition rate depends on the annealing temperature. At 70 °C, the transition is very fast, and the rate decreases at 60 °C and 50 °C. What's more, this transition can even occur very slowly at room temperature. The low transition rate at room temperature makes it possible for future characterization of the chain mobility via solid state NMR. The above results confirm that the transformation is a kinetic solid–solid transition process and does not have a defined transition temperature.

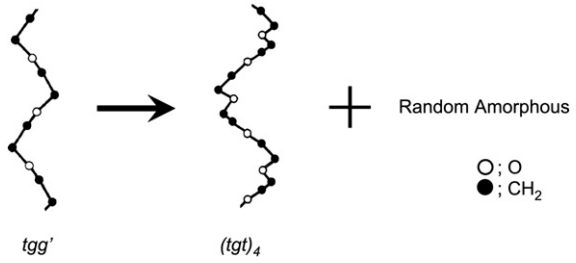

Fig. 10. The sketch map of the conformation change of PEO chains during the solid–solid transition.

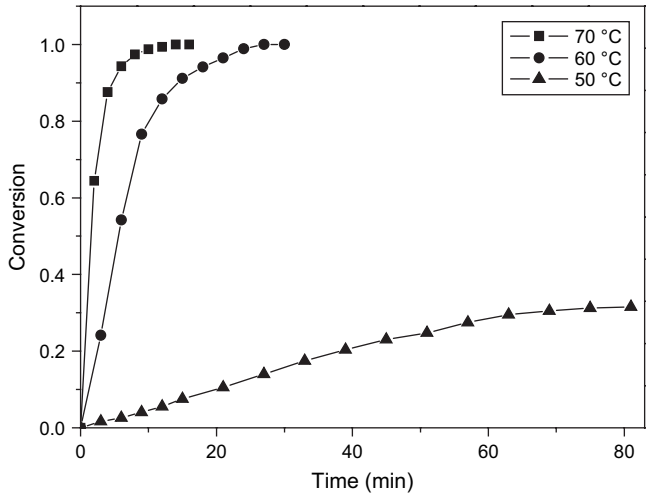

Fig. 11. The conversion from the metastable tetragonal to the stable trigonal IC at 50 °C (▲), 60 °C (●), and 70 °C (■) measured by FTIR, respectively.

To determine the kinetics of the transition, the following equation was used:

$$\frac{dA}{dt^n} = -kA \tag{1}$$

where A is the area of the IR band at 1307 cm^{-1}, n is the exponent, and k is the rate constant depending on the temperature. To obtain n and k, we integrate Eq. (1) to get a double logarithmic equation, the well-known Avrami equation [30]:

$$\log\left[-\ln\left(\frac{A_t - A_\infty}{A_0 - A_\infty}\right)\right] = \log k + n\log t \tag{2}$$

where A_0, A_t and A_∞ is the area of the IR band at time *0*, *t* and ∞, respectively.

Experimental data for Eq. (2) at different temperatures are plotted and presented in Fig. 12. The calculated results are listed in Table 1. The exponent n is around 1 and the rate constant k increases sharply with annealing temperature. Arrhenius equation is employed to get the activation energy of the solid–solid transition:

$$k_T = k_0 \exp\left(-\frac{E}{RT}\right) \tag{3}$$

$$\log k_T = \log k_0 - \frac{E}{2.303RT} \tag{4}$$

where k_T is the rate constant at the temperature T and E is the activation energy of transition. Plot of Eq. (4) is presented in Fig. 13. The activation energy is calculated to be 222 kJ/mol. Assuming hydrogen bonding energy in the tetragonal IC is about 20 kJ/mol, the transition occurs with cooperative disruption of at least 10 hydrogen bonds. Namely, the *tgg′* PEO chains can only transform into the *tgt* conformation along with disruption of the surrounding urea channels.

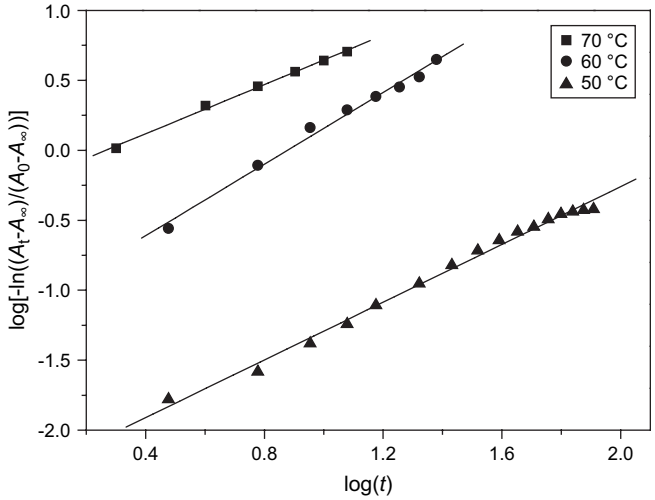

Fig. 12. Plots of $\log[-\ln((A_t-A_\infty)/(A_0-A_\infty))]$ vs. $\log(t)$ for transition process. A_0, A_∞, and A_t are the initial area, final area, and area at time t of peak 1307 cm^{-1}, respectively.

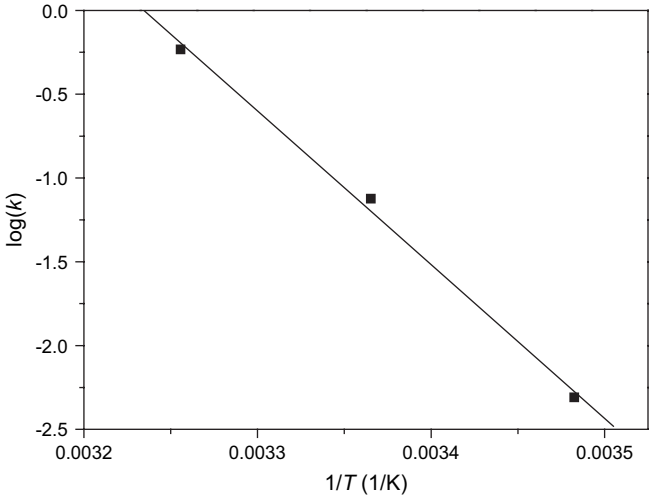

Fig. 13. Plots of $\log(k)$ vs. $1/T$ for transition process. k is the transition rate at temperature T.

3.4. Mobility of the nanoconfined PEO chains

High-resolution solid state ^{13}C CP/MAS/DD (cross-polarization, magic-angle spinning, dipolar decoupling) NMR is a powerful technique to determine the mobility of polymer chains. The spin-lattice relaxation times in the rotating ($T_{1\rho}$ (^1H)) and laboratory frames (T_1 (^{13}C)) have been demonstrated to be sensitive to molecular motions at several tens of kHz and several hundreds of MHz.

The CP/MAS ^{13}C NMR spectra of pure PEO (a), the metastable PEO–urea IC (b), the stable PEO–urea IC (c), and the transformed product of the metastable IC after annealing at 70 °C overnight (d) are shown in Fig. 14. A resonance peak at about 163.7 ppm in spectrum (b) is assigned to carbon of urea in the tetragonal crystal lattice, which is slightly shifted to 163 ppm in spectra (c) and (d). The resonance peak of methylene carbon of PEO appeared at 71.0 ppm for neat crystallized PEO, 70.2 ppm for the metastable IC, and 70.0 ppm for the stable IC and the transformed product of metastable IC. The bulk PEO spectrum shows a resonance peak containing narrow and broad components, which corresponds to the presence of amorphous and crystalline PEO, respectively. The "upfield" shift of PEO line in the PEO–urea IC is similar to that occurred in the PEO–hydroxybenzene ICs [31], resulting from hydrogen bonding between O of PEO and H of urea. Variation of the chemical shift of PEO reveals that the trigonal IC exhibited stronger hydrogen bonding between PEO and urea than the tetragonal form. The magnified resonance lines of urea in the two types of ICs are presented in Fig. 15.

Table 1
Values of n and k for the transition kinetics determined from real-time FTIR results

	Temperature (°C)		
	50	60	70
n	1.03	1.28	0.88
k	0.0047	0.0753	0.5843

"Upfield" shift of the resonance line of the carbonyl group indicates that the stable trigonal form possesses stronger hydrogen bonding than the metastable tetragonal form, similar to the case of starch/poly(sodium acrylate) [32].

Table 2 shows ^{13}C T_1 for the four samples at room temperature, which reflects the local molecular motions at the frequency region of several hundreds of MHz [33]. It is revealed that PEO in the ICs possessed slower molecular motion than the neat amorphous PEO but faster than the neat crystalline PEO, which agrees with the trend reported by Tonelli et al. [1]. For the ICs, the PEO chains in the tetragonal form show depressed local molecular motion than those in the trigonal form, which may be attributed to the different channel size and the different chain conformation as mentioned above. Annealing of the metastable tetragonal IC at 70 °C overnight produced the transformed product with T_1 (^{13}C) of 0.71 s, an intermediate value between that of the trigonal IC (0.91 s) and the neat amorphous PEO (0.61 s). Consequently, solid state ^{13}C NMR determination further supports the above

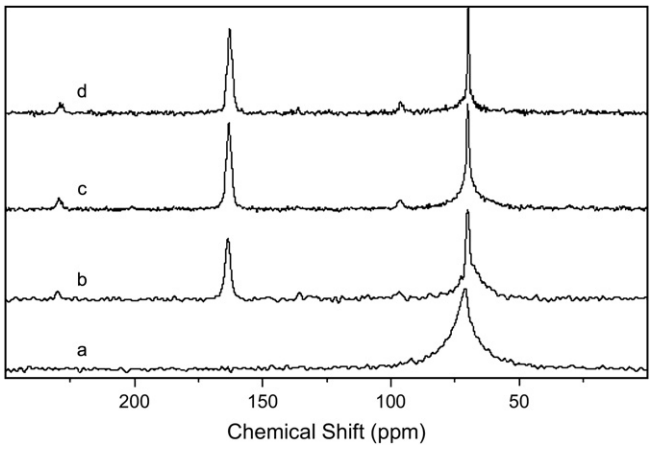

Fig. 14. CP/MAS ^{13}C NMR spectra of (a) pure PEO; (b) the metastable tetragonal PEO–urea IC; (c) the stable trigonal IC, and (d) the transformed product after annealing of (b) at 70 °C overnight.

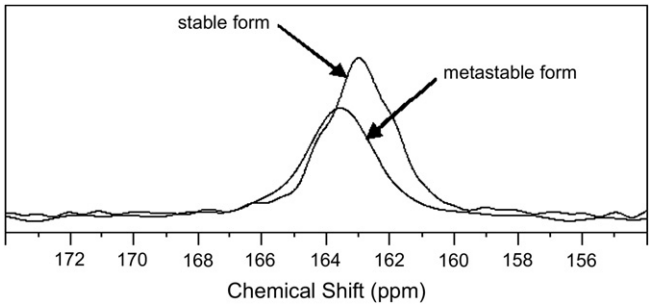

Fig. 15. Resonance lines of urea in the stable trigonal form and the metastable tetragonal form.

Table 2
T_1 (^{13}C) for neat crystallized PEO, the tetragonal IC, the trigonal IC, and the transformed product at room temperature

	Neat PEO	Tetragonal IC	Trigonal IC	Annealing of the tetragonal IC at 70 °C
T_1 (^{13}C) (s)	3.22 (crystalline), 0.61 (amorphous)	1.59	0.91	0.71

proposition that annealing of the tetragonal IC leads to transition to the trigonal IC and some amorphous PEO chains escaped from the urea clathrate nanochannels, as schemed in Fig. 10.

The rotational isomeric state description for amorphous PEO suggests that the energy of *gauche* O–CH_2–CH_2–O is 400 cal/mol greater than that of *trans* conformation [34–36]. Why do PEO chains in the tetragonal IC adopt the former conformation? It may be due to the following reasons: in the melt, PEO chains adopt *gauche* O–CH_2–CH_2–O conformation due to the intramolecular O···H attraction effect [28]. When the IC melt was isothermally crystallized at temperatures higher than 70 °C, the components had enough mobility to form the conformations with strong intermolecular hydrogen bonding between O of PEO and H of urea, thus producing the trigonal form with the minimum free energy. When the IC melt was quenched to temperatures lower than 70 °C, the tetragonal IC possessed the PEO conformation similar to that in the melt PEO (predominantly *tgg′*) [28], so it showed a higher crystallization rate than the stable IC with a different PEO conformation. Consequently, at lower crystallization temperatures, the tetragonal form predominated due to the kinetic effect. Due to the narrow channel size of the urea clathrates (about 7 Å), transition of the PEO chain conformation from *tgg′* to *tgt* is very slow at room temperature (more than a month for complete transformaion). During annealing of the tetragonal IC at higher temperature, the tetragonal urea channels disrupted, so the PEO chains and urea cooperatively assembled into the stable trigonal form with *tgt* PEO conformation.

3.5. Nonlinear optical response of PEO–urea ICs

Second harmonic generation (SHG) microscopy is a novel method to study the second order nonlinear optical properties of heterogeneous material [37–39], in which two photons at the fundamental frequency ω are converted into one photon at the frequency 2ω. In contrast to the conventional measurement determining only the average SHG intensity in the incident region (usually with a diameter about several millimeters), SHG imaging is capable of obtaining the spatial distribution of SHG response in the material with resolution down to submicrons [40,41]. Thus, dependence of the SHG activity on the crystalline structure of the inclusion compound can be investigated. Different crystalline forms of PEO–urea IC display different SHG activity, as demonstrated in Fig. 16. In the SHG micrograph, the brighter region indicates stronger second order optical activity. It is shown that the trigonal IC (zone 2) reveals stronger SHG activity than the tetragonal form (zone 1), which can be attributed to the stronger hydrogen bonding in the former based on the report

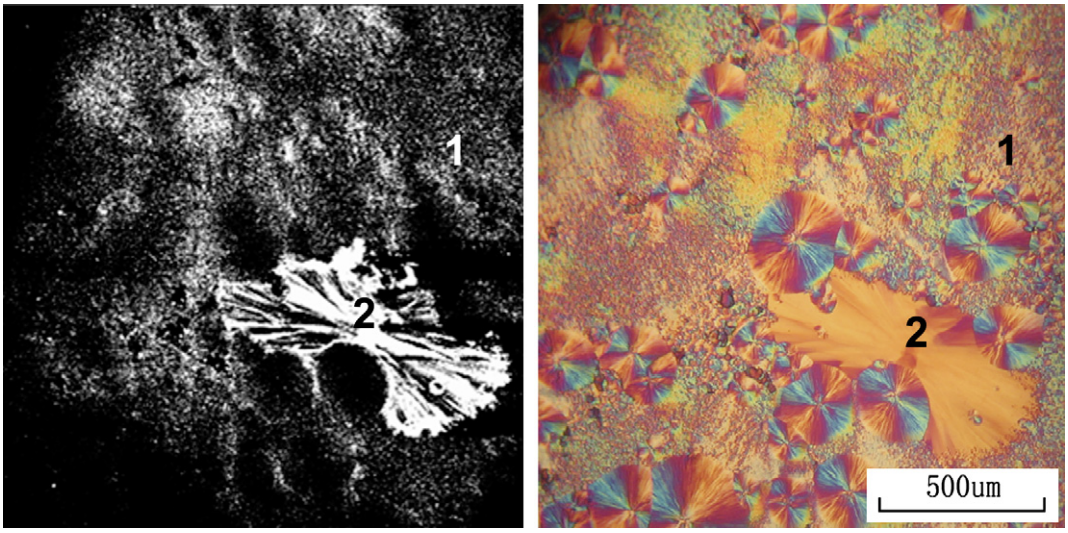

Fig. 16. Second harmonic generation micrograph (left) and polarized optical micrograph (right) of the tetragonal (the small crystal grains) indicated by zone 1 and the trigonal form PEO–urea IC indicated by zone 2 in the same film.

that in some organic crystals, hydrogen bonding enhances the hyperpolarizability and thus the SHG activity [42–44].

4. Conclusion

The PEO–urea ICs formed from melt can adopt two crystalline modifications: trigonal or tetragonal, depending on the crystallization temperature. FTIR and Raman spectroscopies reveal that the PEO chains in the trigonal modification appear with the previously reported *tgt* O–CH_2–CH_2–O conformation, while those in the tetragonal modification possess predominantly *tgg′* conformation. The transition of PEO–urea IC from the metastable tetragonal form to the stable trigonal form was observed via real-time FTIR and WAXD. During the conversion, the PEO *tgg′* conformation in the urea nanochannels change into the *tgt* and the random amorphous conformation. It is a solid–solid transition process with the rate depending on the annealing temperature. Furthermore, solid state ^{13}C NMR was carried out to measure the molecular mobility in the ICs indirectly. The laboratory frame spin-lattice relaxation time T_1 (^{13}C) shows that the PEO chains in the tetragonal form show depressed local molecular motion than those in the trigonal form; nonetheless, PEO chains in the two IC forms exhibit decreased chain mobility than the neat amorphous PEO, but enhanced mobility than the neat crystalline PEO. Second harmonic generation microscopy reveals that the trigonal IC exhibits stronger nonlinear optical activity than the tetragonal IC due to the stronger hydrogen bonding in the former. All the experimental results demonstrate that hydrogen bonding is the driving force for the transformation of the metastable PEO–urea IC.

Acknowledgement

We are grateful for the financial support from the Open Lab Funds of Tsinghua University, the Key Laboratory of Education Ministry for Optics and Magnetic Resonance Spectroscopy and the National Natural Science Foundation of China (Grant Nos. 20334020, 60138010, 20504019).

References

[1] Lu J, Mirau PA, Tonelli AE. Prog Polym Sci 2002;27:357–401.
[2] Ohmura M, Kawahara Y, Okude K, Hasegawa Y, Hayashida M, Kurimoto R, et al. Polymer 2004;45:6967–75.
[3] Volel M, Armand M, Gorecki W, Saboungi M-L. Chem Mater 2005;17:2028–33.
[4] Girardeau TE, Leisen J, Beckham HW. Macromol Chem Phys 2005;206:998–1005.
[5] Tonelli AE. Polymer 1994;35:573–9.
[6] Reisner W, Morton KJ, Riehn R, Wang YM, Yu ZN, Rosen M, et al. Phys Rev Lett 2005;94:196101-1–196101-4.
[7] Iwamoto R, Wakano H. J Am Chem Soc 1976;98:3764–8.
[8] Yokoyama M, Ishihara H, Iwamoto R, Tadokoro H. Macromolecules 1969;2:184–92.
[9] Harris KDM, Thomas JM. J Chem Soc Faraday Trans 1999;86:2985–96.
[10] Suehiro K, Nagano Y. Makromol Chem Rapid Commun 1983;4:137–40.
[11] Vasanthan N, Shin ID, Tonelli AE. Macromolecules 1994;27:6515–9.
[12] Howe C, Vasanthan N, MacClamrock C, Sankar S, Shin ID, Simonsen IK, et al. Macromolecules 1994;27:7433–6.
[13] Vasanthan N, Shin ID, Tonelli AE. Macromolecules 1996;29:263–7.
[14] Bogdanov BG, Michailov M, Uzov CV, Gavrailova GG. J Polym Sci Part B Polym Phys 1994;32:387–94.
[15] Suehiro K, Nagano Y. Makromol Chem 1983;184:669–74.
[16] Suehiro K, Urabe A, Yoshiake Y, Nagano Y. Makromol Chem 1984;185:2467–73.
[17] Hikichi K, Oka D, Shibata T, Uzawa J. Polym J 1999;31:692–4.
[18] Tonelli AE. Polym Int 1997;43:259–309.
[19] Smith AE. Acta Crystallogr 1952;5:224–35.
[20] Chenite A, Brisse F. Macromolecules 1991;24:2221–5.
[21] Bogdanov BG, Michailov M, Uzov C, Gavrailova G. Macromol Chem Phys 1994;195:2227–31.
[22] Marcos JI, Orlandi E, Zerbi G. Polymer 1990;31:1899–903.
[23] Marentette JM, Brown GR. Polymer 1998;39:1405–14.
[24] Jeevanandam P, Vasudevan S. Chem Mater 1998;10:1276–85.
[25] Aranda P, Ruiz-Hitzky E. Appl Clay Sci 1999;15:119–35.
[26] Leroux F, Aranda P, Besse JP, Ruiz-Hitzky E. Eur J Inorg Chem 2003;6:1242–51.
[27] Takahisa Y, Sumita I, Tadokoro H. J Polym Sci Polym Phys Ed 1973;11:2113–22.
[28] Yang XZ, Su ZH, Wu DC, Hsu SL, Stidham HD. Macromolecules 1997;30:3796–802.
[29] Yoshida H, Matsuura H. J Phys Chem A 1998;102:2691–9.
[30] Avrami M. J Chem Phys 1940;8:212–24.
[31] Spěváček J, Paternostre L, Damman P, Draye AC, Dosière M. Macromolecules 1998;31:3612–6.
[32] Kong XX, Xu K, Wang PX, Chen Q. Chem J Chin Univ 2005;26:1739–42.
[33] Zhao HP, Lin WX, Yang G, Chen Q. Eur Polym J 2005;41:2354–9.
[34] Mark JE, Flory PJ. J Am Chem Soc 1965;87:1415–23.
[35] Abe A, Tasaki K. Macromolecules 1986;19:2647–8.
[36] Harris DJ, Bonagamba TJ, Schmidt-Rohr K. Macromolecules 1999;32:6718–24.
[37] Hermann DS, Rudquist P, Lagerwall ST, Komitov L, Stebler B, Lindgren M, et al. Liq Cryst 1998;24:295–310.
[38] Watanabe J, Hirose Y, Tokita M, Watanabe T, Miyata S. Macromolecules 1998;31:5937–9.
[39] Xu J, Bao J, Guo BH, Ma H, Yun TL, Gao L, et al. Polymer 2007;48:348–55.
[40] Campagnola PJ, Millard AC, Terasaki M, Hoppe PE, Malone CJ, Mohler WA. Biophys J 2002;82:493–508.
[41] Willams RM, Zipfel WR, Webb WW. Biophys J 2005;88:1377–86.
[42] Moolya BN, Jayarama A, Sureshkumar MR, Dharmaprakash SM. J Cryst Growth 2005;280:581–6.
[43] Wu KC, Snijders JG, Lin CS. J Phys Chem B 2002;106:8954–8.
[44] Skwara B, Gora RW, Bartkowiak W. Chem Phys Lett 2005;406:29–37.